This paper has been accepted for publication in *Géotechnique*

Strength-dilatancy and critical state behaviours of binary mixtures of graded sands influenced by particle size ratio and fines content

Yuksel Yilmaz, Ph.D.[1]; Yibing Deng, Ph.D.[2]; Ching S. Chang, Ph.D.[3]; Aydin Gokce, MSc.[4]

[1]Professor (ORCID number 0000-0001-7630-7357), Gazi University, Ankara, Turkey, e-mail: yyuksel@gazi.edu.tr

[2]Research Assistant (ORCID number 0000-0001-5343-1988), University of Massachusetts Amherst, Amherst, MA, USA, e-mail: yibingdeng@engin.umass.edu (Corresponding Author)

[3]Professor (ORCID number 0000-0002-3595-5099), University of Massachusetts Amherst, Amherst, MA, USA, e-mail: cchang@engin.umass.edu

[4]Lecturer (ORCID number 0000-0002-1611-2168), Gazi University, Ankara, Turkey, e-mail: agokce@gazi.edu.tr

Abstract:

Binary granular soil mixtures, as common heterogeneous soils, are ubiquitous in nature and man-made deposits. Fines content and particle size ratio are two important gradation parameters for a binary mixture, which have potential influences on mechanical behaviours. However, experimental studies on drained shear behaviour considering the whole range of fines content and different particle size ratios are scarce in the literature. For this purpose, we performed a series of drained triaxial compression tests on dense binary silica sand mixtures with 4 different particle size ratios to systematically investigate the effects of fines content and particle size ratio on the drained shear behaviours. Based on these tests, the strength-dilation behaviour and critical state behaviour were examined. It was observed that both fines content and particle size ratio have significant influence on the stress-strain response, the critical state void ratio, the critical state friction angle, the maximum dilation angle, the peak friction angle, and the strength–dilatancy relation. The underlying mechanism for the effects of fines content and particle size ratio was discussed from the perspective of the kinematic movements at particle level.

Keywords: Laboratory tests; Sands; Particle-scale behaviour; Shear strength; Deformation

1. Introduction

Heterogeneous soils are ubiquitous in nature and man-made deposits. These soils are generally composed of a binary mixture of large particles and small particles, such as gravel-sand mixtures and sand-silt mixtures, which are commonly encountered in dams, fills, fault zones, and landslides. The mechanical behaviour of binary soil mixtures have been found very different from that of uniform soil (Carraro et al., 2009; Chang & Phantachang, 2016; Derkaoui et al., 2016; Jehring & Bareither, 2016; Salgado et al., 2000).

Fines content and particle size ratio are two important gradation parameters for a binary mixture, which distinguished mixtures from uniform soils. Thus, it is important to understand the effects of fines content and particle size ratio on the mechanical behaviour of a binary soil mixture.

Many efforts have been made to study the behaviour of binary soil mixtures. The effect of fines content on critical void ratio have been studied using the experimental results by many investigators (e.g., Carrera et al. 2011; Dash and Sitharam 2011; Kwa and Airey 2016; Naeini and Baziar 2004; Papadopoulou and Tika 2008; Thevanayagam et al. 2002; Yang 2004; Zlatović and Ishihara 1995). All these results show significant effects of fines content on critical state void ratio, which decreases as fine content increases from zero to about 30%. Then, as the fines content continues to increase, the void ratio increases. This trend is very useful for the evaluation of engineering properties of silty sands using the critical state soil mechanics framework.

The effect of fines content on dilatancy for silty sands is usually studied by drained triaxial tests. However, there are limited studies in this area (Carraro et al., 2009; Salgado et al., 2000; Xiao et al., 2017; Patil et al., 2018). Also, in these studies, the fines contents were less than 30%. Among these studies some investigators stated that the Bolton's dilatancy equation proposed for clean sand could still be used for silty sands (Xiao et al., 2017) with the same parameter b: $b = (\phi_p - \phi_{cv})/\psi_p$, where ϕ_p, ϕ_{cv}, and ψ_p are the peak friction angle, critical state friction angle and maximum dilation angle, respectively. b is a dilatancy parameter of 0.436 for Fujian sand with non-plastic fines. This statement needs to be verified for the case of higher fines content (i.e., greater than 30%).

The effect of fines content on the critical state friction angle have been studied by both drained and undrained triaxial tests. Some investigator found that the critical state friction angle varies with fines content (Murthy et al., 2007; Salgado et al., 2000; Xiao et al., 2017), while others found that the critical state friction angle is independent of fines content (Bouckovalas et al., 2003; Ni et al., 2004; Rahman et al., 2014).

Based on these investigations, fines content has been found to have significant influence on the soil behaviours associated with void ratio such as maximum and minimum densities, critical state line, and normal compression line, etc. For each soil behaviour, investigations indicated the existence of a transitional or threshold fines content, which is considered to be the boundary between the behaviour dominated by the coarser particles and the behaviour dominated by the finer particles in binary mixtures (Thevanayagam et al., 2002; Yang et al., 2006; Chang and Meidani, 2013; Zuo and Baudet, 2015). The concept of transitional fines content has been broadly accepted in soil mechanics. The transitional fine content is different for different soil behaviour, usually varies between 20% and 50%, as discussed by Zuo and Baudet (2015). The existence of transitional fines content, however, has not been discussed in the literature for strength-dilatancy behaviour, which needs to be investigated.

Besides fines content, the particle size ratio is also an important factor for a binary mixture. However, until now, very few studies are available in the literature addressing the effect of particle size ratio on critical state behaviour and strength-dilatancy behaviour. Although there are abundant drained triaxial test results on silty sands in the literature, these test results cannot be used to evaluate the effect of particle size ratio because the particle size ratio cannot be isolated from other factors. As far as the authors are aware, there have been only a few studies on particle size ratio using discrete element simulations (Ueda et al., 2011; Zhou et al., 2016; Zhu et al., 2020). But, in the literature, there is no attempts which have been made in real soil mixtures or glass beads mixtures to study the effect of particle size ratio on critical state behaviour and stress-dilatancy behaviour.

The main objective of this work is to investigate the effects of fines content and particle size ratio on critical state behaviour and strength-dilatancy behaviour of binary granular soil mixtures. For this purpose, a series of drained triaxial compression tests at a constant confining stress (200 kPa) were conducted on dense binary silica sand mixtures. These binary mixtures were made up of 5 size classes of sand particles with various fines contents so that the factor of particle size ratio can be isolated. This paper is organized as follows. The testing program and test results are firstly presented. Then the test results are analyzed to observe the effects of fines content and particle size ratio on the critical state and the strength-dilatancy characteristics of the mixed graded material. The observed patterns are discussed and the underlying mechanism for the influences of fines content and particle size ratio on drained shear behaviour is discussed.

2. Testing Program

2.1 Testing material

Pasabahce silica sand (herein referred to as silica sand) were selected to use in this experimental study. The silica sand is formed as a result of disintegration of magmatic metamorphic rocks being rich in quartz. The fluvial transportation brought it to actual deposit in Istanbul, Turkey. By sieving the silica sand, five graded uniform silica sands were obtained and used in this experimental study, i.e., #16-#18, #30-#50, #50-#80, #100-#120, and #120-#200, each of which is the upper sieve number and the lower sieve number. The particle size and specific gravity of the samples (obtained by ASTM D854-14) are listed in Table 1. A qualitative look at the shape and surface texture of the individual sand grains were determined using the method of 2-D microscopy. Fig. 1 shows a series of micrographs of some grains from the silica sands used in this study. The sand grains are mostly sub-angular. Based on these micrographs, Roundness (R_W) for each uniform sand was calculated using its definition proposed by Wadell (1935) and listed in Table 1. The minimum void ratio $e_{\min}$ (maximum index density) and the maximum void ratio $e_{\max}$ (minimum index density) of each uniform silica sand were determined according to Method 2A of ASTM D4253 (ASTM D4253-00, 2006) and Method B of ASTM D4254 (ASTM D4254-00, 2006), respectively. The minimum and the maximum void ratios of samples are tabulated in Table 1.

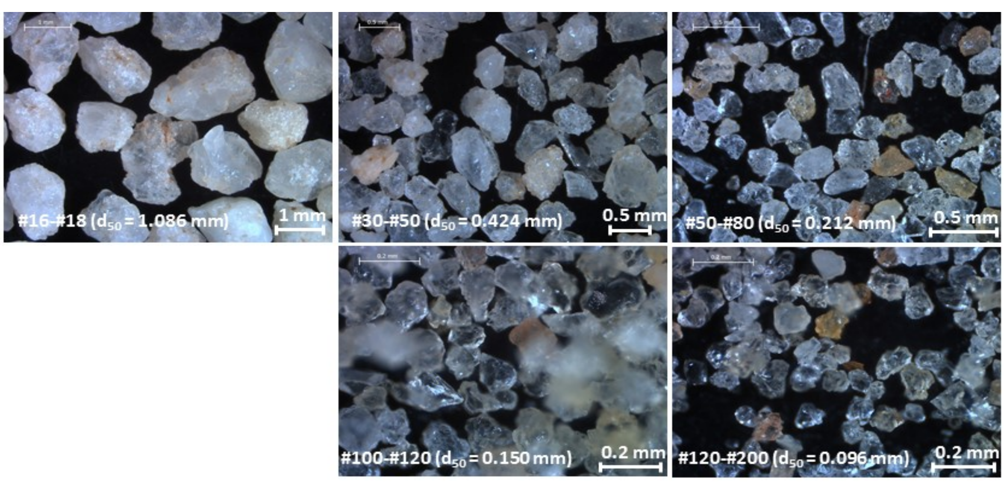

Fig. 1. Micrographs of uniform silica sands of five different particle sizes.

Table 1 Properties of the uniform silica sands of five different particle sizes.

Uniform sand[1]	Notes[2]	d_{50} (mm)	Roundness	G_s	e_{max}	e_{min}
#16 – #18	Medium sand	1.086	0.36	2.624	0.901	0.632
#30 – #50	Medium/Fine sand	0.424	0.26	2.640	0.999	0.698
#50 – #80	Fine sand	0.232	0.17	2.646	1.102	0.786
#100 – #120	Fine sand	0.137	0.18	2.652	1.108	0.778
#120 – #200	Fine sand	0.096	0.23	2.654	1.099	0.717

Note: [1]No.# - No.# are the upper sieve number and the lower sieve number respectively for a uniform sand.
[2]the classification is according to ASTM D422-63 (2007).

To study the effects of fines content and particle size ratio, four series of binary mixtures with four different particle size ratios were prepared by mixing #16-#18 uniform sand with one of the other four uniform sands. Herein, the #16-#18 sand is referred to as "coarse" particles and the other four smaller size sand are referred to as "fine" particle. For each particle size ratio, the series of binary mixture were prepared with fines content $f_c = 0.1, 0.2, 0.3, 0.5, 0.7$. We define fines content as the ratio of the mass of the small particle sand to the total mass of a binary mixture in this study. Particle size ratio is the ratio of the large particle size to the small particle size in a binary mixture. The particle size distributions of binary mixtures with four different particle size ratios are presented in Fig. 2. The minimum void ratio and the maximum void ratio of four series of binary mixtures were determined according to Method 2A of ASTM D4253 (2006) and Method B of ASTM D4254 (2006), respectively. The minimum and the maximum void ratios of these binary mixture samples are tabulated in Table 2.

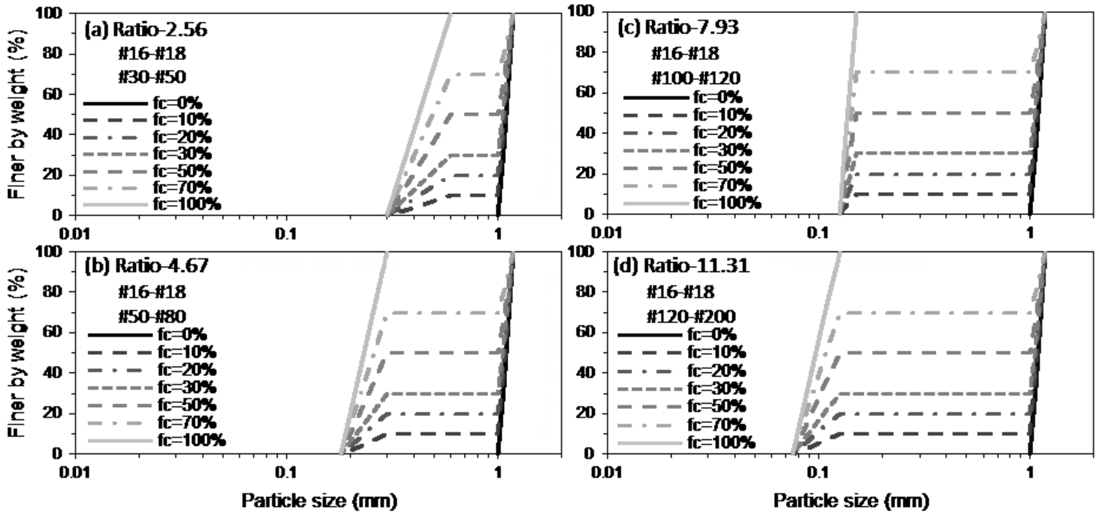

Fig. 2. The grain size distributions of binary mixtures with four different particle size ratios: (a) Ratio-2.56, (b) Ratio- 4.67, (c) Ratio-7.93, and (d) Ratio-11.31

Table 2 List of index properties of tested binary mixtures.

Symbol	Mixture series	Size ratio[1] $\frac{d_{50\_\mathrm{coarse}}}{d_{50\_\mathrm{fine}}}$	f_c (%)	$e_{\max}$	$e_{\min}$
Ratio-2.56	#16-#18 #30-#50	2.56	10	0.874	0.603
			20	0.828	0.566
			30	0.8	0.54
			50	0.802	0.548
			70	0.873	0.620
Ratio-4.67	#16-#18 #50-#80	4.67	10	0.830	0.571
			20	0.734	0.508
			30	0.703	0.491
			50	0.725	0.501
			70	0.858	0.592
Ratio-7.93	#16-#18 #100-#120	7.93	10	0.795	0.547
			20	0.679	0.452
			30	0.635	0.393
			50	0.648	0.463
			70	0.821	0.585
Ratio-11.31	#16-#18 #120-#200	11.31	10	0.797	0.523
			20	0.659	0.408
			30	0.583	0.335
			50	0.600	0.415
			70	0.776	0.517

Note: [1] d_{50_coarse} is the large particle mean size and d_{50_fine} is the small particle mean size.

2.2 Drained triaxial compression testing

A conventional triaxial device was used to study the drained shear behaviour of binary silica sand mixtures. All tests were performed on cylindrical specimens (50 mm in diameter and 100 mm in height) under the confining stress of 200 kPa. A total number of 25 triaxial tests were performed. All specimens were prepared by the moist tamping method with the under-compaction technique introduced by Ladd (1978). The moist soil with a moisture content of 5% was placed in the split mold and then compacted to a specified density in five layers. A 3% under-compaction ratio, defined as the difference in density between successive layers, was used in the sample preparation to improve the uniformity within specimens. The moist tamping method is able to minimize particle segregation because of capillarity. Because of the advantage in creating uniform samples and avoiding particle segregation, the moist tamping method using under-compaction is preferred in the sample preparation for sand-silt mixtures (e.g., Huang et al., 2004; Wei and Yang, 2019; Yang et al., 2006).

Note that the minimum and the maximum void ratios of the samples were obtained by using dry sand (according to ASTM D4253-00 (2006) and ASTM D4254-00 (2006)). The initial void ratios e_0 of all samples after preparation using the moist tamping method were plotted in Fig. 3, compared with the measured values of e_{min} and e_{max}. As shown in Fig.3, the value of e_0 for all samples is nearly the same as that of e_{min}, which indicates that all samples have same initial relative density of around 97%.

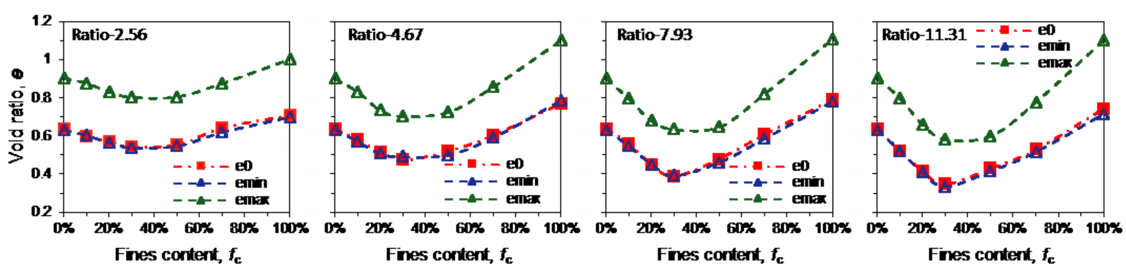

Fig. 3. The initial void ratios e_0 of all samples.

After the sample preparation and installation into the triaxial cell, the specimen was saturated by flushing with carbon dioxide gas and then flushing with deaired water, followed by backpressure saturation to achieve a value of Skempton's B parameter of greater than 0.96. Then the specimen was isotropically consolidated under the desired effective confining stress. After consolidation, the specimen was sheared until failure by compressing the specimen at a constant vertical displacement rate of 0.2 mm/min under the confining stress. All samples were under a drained condition during the course of shearing. Particle breakage was not observed in any test. The results of the triaxial tests are summarized in Table 3.

Major and minor principal effective stresses are denoted by σ_1' and σ_3'. Axial and volumetric strains are denoted by ε_a and ε_v. Contractive strains are considered positive and dilative strains are considered negative.

<**Table 3** Summary results of drained triaxial compression tests on the specimens of binary silica sand mixtures of various fines contents for four different particle size ratios.>

Samples	Fines content	Void ratio					Shearing				
		Initial	Consoli-dation	Onset of dilatancy	Peak stress	Critical State (CS)	Strain at peak stress		Peak friction angle	Max. dilatancy angle	CS friction
							Axi	Vol.			
	f_c	e_0	e_c	e_f	e_p	e_{cs}	ε_a	ε_v (%)	ϕ_p (°)	ψ_p (°)	ϕ_{cv}
#16-#18	-	0.6	0.621	0.617	0.663	0.727	9.5	-2.6	38.0	11.0	32.8
#16-#18	10	0.5	0.583	0.579	0.619	0.692	10.	-2.5	36.9	9.3	31.6
	20	0.5	0.558	0.553	0.584	0.643	10.	-1.7	36.0	7.7	31.5
#30-#50	30	0.5	0.531	0.527	0.561	0.611	8.2	-1.5	37.6	9.0	33.6
	50	0.5	0.544	0.541	0.575	0.631	8.3	-2.0	38.1	9.9	33.6
(Ratio-2.56)	70	0.6	0.631	0.626	0.655	0.713	9.0	-1.6	37.0	8.3	33.1
	100	0.7	0.700	0.696	0.746	0.805	9.4	-2.7	39.0	11.7	33.6
#16-#18	10	0.5	0.562	0.558	0.603	0.665	12.	-2.5	36.2	8.5	31.7
	20	0.5	0.499	0.494	0.517	0.569	9.0	-1.3	36.4	7.1	31.9
#50-#80	30	0.4	0.461	0.456	0.471	0.503	8.9	-0.7	36.6	5.2	32.8
	50	0.5	0.512	0.508	0.528	0.559	8.7	-0.9	36.8	6.6	33.7
(Ratio-4.67)	70	0.6	0.595	0.591	0.625	0.690	8.9	-2.1	39.2	9.6	34.5
	100	0.7	0.756	0.752	0.812	0.894	9.2	-3.2	40.0	12.3	35.0
#16-#18	10	0.5	0.542	0.535	0.561	0.601	11.	-1.5	35.2	8.0	31.8
	20	0.4	0.435	0.428	0.464	0.500	14.	-1.8	34.9	6.7	32.1
#100-#120	30	0.3	0.376	0.370	0.375	0.408	6.5	-0.03	35.9	4.6	31.3
	50	0.4	0.470	0.465	0.484	0.525	7.9	-1.2	38.4	8.2	34.8
(Ratio-7.93)	70	0.6	0.598	0.593	0.617	0.677	7.3	-1.2	38.1	10.1	33.3
	100	0.7	0.784	0.780	0.829	0.903	7.8	-2.0	39.9	12.6	35.2
#16-#18	10	0.5	0.505	0.502	0.550	0.597	11.	-3.0	38.1	11.0	33.0
	20	0.4	0.404	0.402	0.433	0.484	9.5	-1.7	36.9	7.1	31.9
#120-#200	30	0.3	0.339	0.333	0.339	0.356	7.8	-0.03	36.8	4.0	31.7
	50	0.4	0.422	0.420	0.435	0.459	5.6	-0.9	38.4	9.2	33.1
(Ratio-11.31)	70	0.5	0.523	0.519	0.544	0.621	5.7	-1.32	40.1	12.0	35.2
	100	0.7	0.734	0.730	0.770	0.865	7.0	-2.1	41.1	13.3	35.1

3. Test Results

3.1 Stress-strain and volumetric change responses

Fig. 4 shows deviatoric stress q ($q = \sigma_1' - \sigma_3'$) and volumetric strain (ε_v) versus axial strain (ε_a) relationships for these four series of binary mixtures, respectively. As shown in Fig. 4, all specimens exhibited a softening behaviour in the plot of stress versus strain and a dilative behaviour in the plot of volumetric strain versus axial strain. Following the initial slight contraction at a small axial strain, dilation then commences. After the onset of dilation, it continues during shearing until the deviatoric stress mobilizes to the peak value. After the peak deviatoric stress, the stress decreases and appears to approach a stable value indicating that a critical state will be reached at larger strains.

Fig. 4 shows that fines content affects peak shear strength and volumetric response. There is a general trend of the effect of f_c on peak shear strength: at low f_c, the peak strength is reduced with an increase of f_c until a particular f_c termed transitional fines content f_{th} is reached; After that a further increase in f_c results in an increase of the peak strength. Herein, the transitional fines content f_{th} is defined as the point at which the trend reverses.

Considering volumetric response, it was observed that the curve of ε_v vs. ε_a moves upwards with increase of f_c until reaching a transitional fine content f_{th}, after that the curve tends to move downwards with further increasing f_c. For example, for Ratio-4.67 mixtures, the curve moves upwards from the curve of $f_c = 0$ to the top one ($f_c = 30\%$) with increase of f_c. Then, with further increasing f_c, the curve moves downwards from the top one to the lowest one ($f_c = 100\%$). This observation implies that increasing f_c could suppress dilation when $f_c < f_{th}$, on the other hand, increasing f_c could promote dilation when $f_c > f_{th}$.

Fig. 4 shows particle size ratio has significant influence on the characteristics of the stress-strain curve for high f_c samples (i.e. $f_c \geq 50\%$). However, particle size ratio has little influence for low f_c samples ($f_c < 30\%$).

It was observed that for high f_c samples, increasing particle size ratio intensifies the post peak softening of the stress-strain curves (i.e., brittle characteristic). It can be found that for the samples of Ratio-11.31 at high f_c, the strain softening is so intense that it exhibits a collapse behaviour of the stress-strain curves. Correspondingly, visible shear bands were observed in these tests. For low f_c samples, however, increasing particle size ratio has little influence on the degree of post peak softening of the stress-strain curve.

The reason could be that, for low f_c, large particle network dominates the behaviour. The large particles are of same size in the mixtures of four different particle size ratios. On the other hand, for high f_c, small particle matrix dominates the behaviour. And the sizes of small particles are dramatically different in the mixtures of four size ratios.

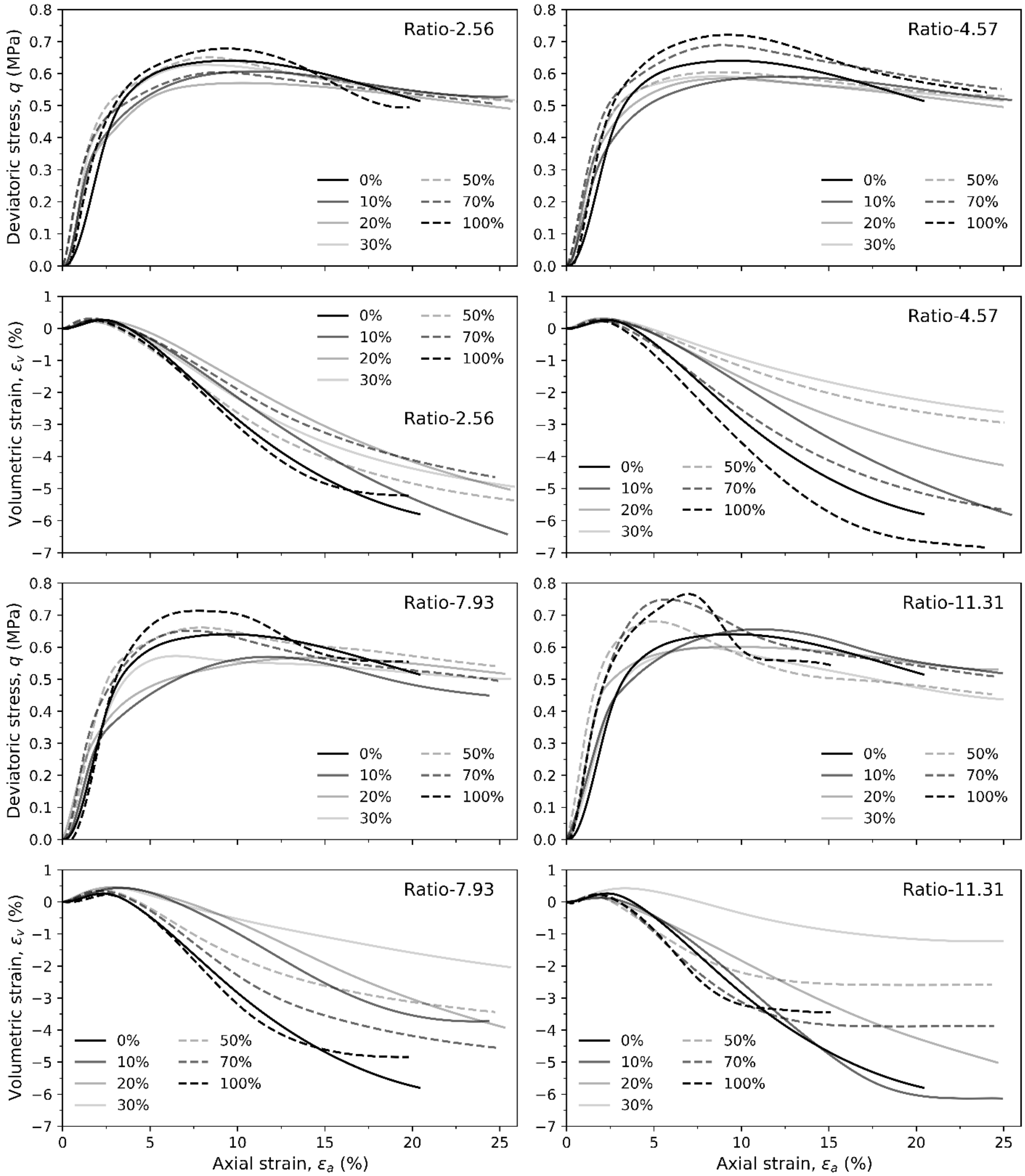

Fig. 4. Experimental results of the drained triaxial compression tests on binary mixtures of various fines contents and particle size ratios.

3.2 Stress-dilatancy plot

The stress- dilatancy evolution of mixtures is presented in Fig. 5 for each particle size ratio. For clarity, the data for $f_c \leq f_{th}$ and $f_c \geq f_{th}$ are separately shown in Fig. 5.

All stress-dilatancy plots show that there is an initial nonlinear part of the curve before the stress ratio η ($\eta = q/p'$) has reached around $\eta = 0.8$. Then, a consistent increase of dilatancy D ($D = -d\varepsilon_v/d\varepsilon_q$) with an increase in the stress ratio $\eta = q/p'$, prior to the maximum dilatancy. Here, p' is mean effective stress ($p' = (\sigma_1' + 2\sigma_3')/3$) and ε_q is deviator strain ($\varepsilon_q = \varepsilon_a - \varepsilon_v/3$).

Once D reaches a peak (D_{max}), the curves go backwards, yielding a "hook" in the curve as it approaches to the critical state. This behaviour is in agreement with that of Erksak sand (Been and Jefferies, 2004). Li and Dafalias (2000) proposed a model to capture this behaviour.

As shown in Fig. 5, D_{max} and the corresponding peak stress ratio η_{max} on the stress-dilatancy plot vary with different f_c. For $f_c \leq f_{th}$, addition of fine particle reduces the values of D_{max} and the corresponding η_{max}. For $f_c \geq f_{th}$, further increasing f_c rises the values of D_{max} and the corresponding η_{max}. This behaviour agrees with the effect of fines content on peak shear strength and volumetric response mentioned previously. The measured values of D_{max} and the corresponding η_{max} will be used to calculate the maximum dilation angle ψ_p and the peak friction angle ϕ_p, respectively, which will be discussed in the later section.

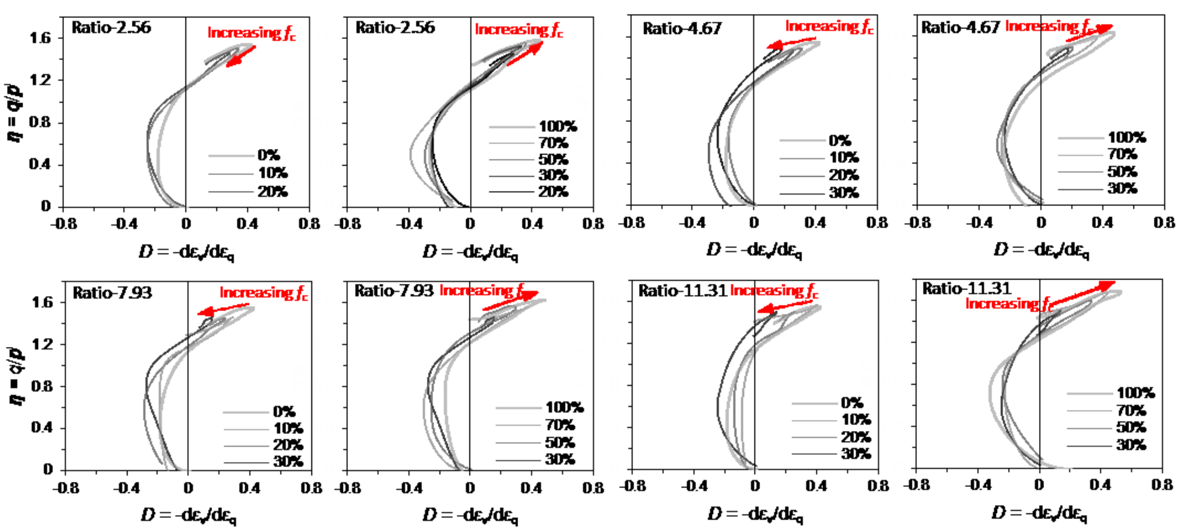

Fig. 5. The stress-dilatancy plots for binary mixtures of various fines contents and particle size ratios.

4. Analyses of Test Results

Based on the test results, the critical state void ratio, the critical state friction angle, the maximum dilation angle, and the peak friction angle can be obtained. In this section, we will discuss the effects of fines content and particle size ratio on the critical state void ratio, the critical state friction angle, the maximum dilation angle, the peak friction angle, and the strength–dilatancy relation.

4.1 Determination of critical state

Critical state (CS) is defined as the state at which the soil continues to deform in shear at constant stress (effective mean stress and shear stress) and constant void ratio (Roscoe et al., 1958). In this study, the triaxial tests were performed up to the maximum axial strain in the apparatus (25%). At this strain, however, the samples have not yet reached the critical state. As suggested by Murthy et al. (2007) and Carrera et al. (2011), it is necessary to extrapolate the stress–strain data to reach the critical state. An extrapolation method, used by Indraratna et al. (2014) and Xiao et al. (2016), was applied to determine the critical state for our tests. Typical examples for extrapolating the data to critical state are given in Appendix A. The extrapolation is more reliable if localisation has not yet occurred at 25% strain. However, the extrapolation is not reliable if the occurrence of localisation is before 25% axial strain and accompanied with large nonhomogeneous deformation. In our tests, localisation was observed in some samples (9 out of 25), especially the samples with large particle size ratios at very high or very low fines contents. In the other 16 samples (mostly in the transitional region of fines content) localisation was not observed.

For these samples with localisation, the abovementioned method is no longer applicable due to the nonhomogeneous deformation. For these cases with localisation, we have adopted another method suggested by investigators (Harehdasht et al., 2017; Nova, 1982). This method requires multiple test results from the same sample under different confining stresses, instead of a single test, to determine the critical state. Examples using the multiple tests method are given in Appendix A.

4.2 Critical state void ratio

4.2.1 *Background*

The effects of fines content and particle size ratio on random close packing density (corresponding to minimum void ratio) have been studies by McGeary (1961) for steel shots and by Kwan et al. (2013) for glass beads as shown in Fig. 6. Fig. 6 shows that the minimum void ratio of a binary packing depends on fines content f_c and particle size ratio. It was found that the void ratio of binary mixtures decreases with increasing particle size ratio, for any given fines content. Similar results have been found in soil mixtures (Yilmaz, 2009). The relationship between void ratio and f_c has two features: (1) it is a V-shape curve. The lowest void ratio corresponds to a transitional or threshold fines content. (2) the curve has two regions separated by the transitional fines content. The region is coarse-particle dominate region for lower f_c, and fine-particle dominant region for higher f_c.

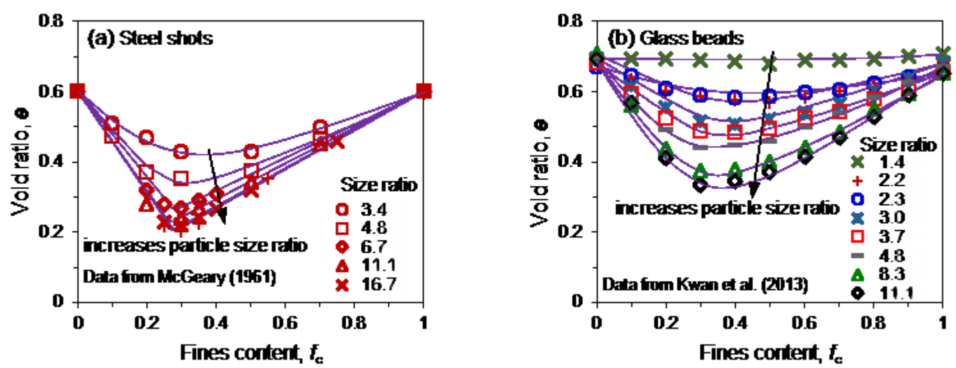

Fig. 6. The minimum void ratios of binary granular mixtures with various particle size ratios: (a) steel shots and (b) glass beads.

The question raised now is whether the special features for minimum void ratio versus f_c are also applicable to critical state void ratio. There have been a lot of experimental data shown that the relationship between e_{cs} and f_c has V-shape characteristic (e.g., Carrera et al., 2011; Dash and Sitharam, 2011; Kwa and Airey, 2016; Naeini and Baziar, 2004; Papadopoulou and Tika, 2008; Thevanayagam et al., 2002; Yang 2004; Zlatović and Ishihara, 1995). For example, Fig. 7 shows the critical void ratios for five different types of sand-silt mixtures. The V-shape characteristics exhibit in the relationship between critical void ratio and fines content.

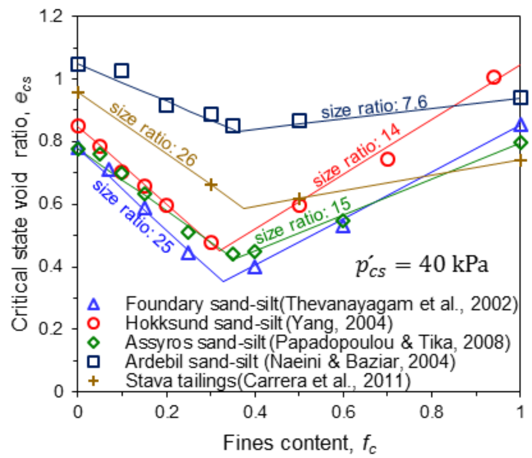

Fig. 7. The critical state void ratios of five different types of sand-silt mixtures with various fines contents.

The plots of critical void ratios under the mean effective stress p'_{cs} of 40 kPa in Fig. 7 were from five types of binary mixtures with different particle size ratios (ranges from 7.6 – 26) (Carrera et al., 2011; Naeini and Baziar, 2004; Papadopoulou and Tika, 2008; Thevanayagam et al., 2002; Yang, 2004). The particle size ratio is 26 for Stava tailings mixtures (Carrera et al., 2011), 25 for Foundry sand-silt mixture (Thevanayagam et al., 2002), 15 for Assyros sand-silt mixtures (Papadopoulou and Tika, 2008), 14 for Hokksund sand-silt (Yang, 2004), and 7.6 for Ardebil sand-silt (Naeini and Baziar, 2004). Fig. 7 shows that there is no trend of the particle size ratio effect on the critical state void ratios of these mixtures, because each mixture has a different material type.

Thus, in order to study the effect of particle size ratio, we construct the binary mixtures using the components of the same material type so that the effect of particle size ratio can be studied with less influence of other unknown factors. For this purpose, a series of drained compression triaxial tests on binary silica sand mixture of the same material type are conducted.

4.2.2 *The results of e_{cs}*

The results of critical state void ratios e_{cs} in this study were plotted in Fig. 8a. The void ratios of samples at the end of testing e_{end} were also plotted in this figure for comparison. The values of e_{cs} and e_{end} for each test are very close. It is observed that the critical state void ratio is dependent on fines content and particle size ratio.

Considering the effect of fines content, the relationship between e_{cs} and fines content is a V-shape character. On the left side, increasing f_c results in decreasing e_{cs} of the binary mixture. On the right side, increasing f_c results in increasing e_{cs} of the binary mixture. This V-shape pattern of fines content influence was also observed in many experiment investigations on silt-sand mixtures (e.g., Carrera et al. 2011; Dash and Sitharam 2011; Kwa and Airey 2016; Naeini and Baziar 2004; Papadopoulou and Tika 2008; Thevanayagam et al. 2002; Yang 2004; Zlatović and Ishihara 1995).

Considering the effect of particle size ratio, as shown Fig. 8a, the curve of e_{cs} vs. f_c moves downwards with increasing particle size ratio. The minimum and maximum void ratios of these mixtures used in this study (listed in Table 2) are plotted in Fig.8b and 8c. Comparing the three void ratios in Fig. 8a, 8b, and 8c, it is observed that the influences of fines content and particle size ratio on e_{cs} are similar to these on e_{max} and e_{min}, even though, the three density states: e_{cs}, e_{max} and e_{min} are achieved by three different mechanical processes. The similarity between the changes of e_{cs} and of e_{min} due to fines content has also been found by other investigators (Chang and Yin, 2011; Chang and Meidani, 2013; Yin et al., 2014).

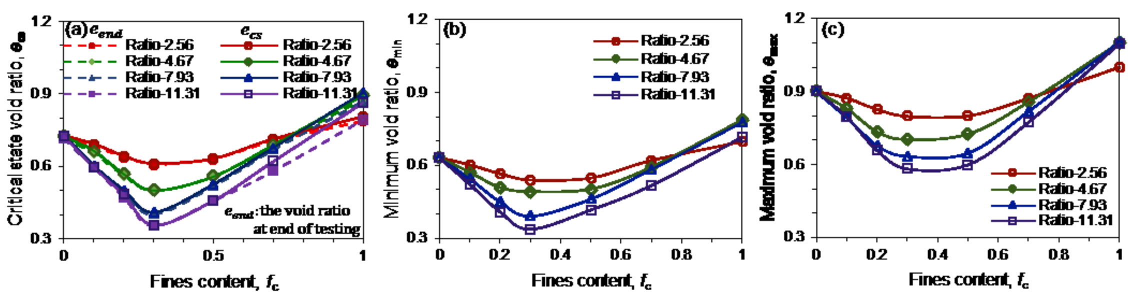

Fig. 8. The effects of fines content and particle size ratio on (a) critical state void ratio, (b) minimum void ratio, and (c) maximum void ratio.

We further investigate the packing potential indices of the three density states. For a system of mixtures (i.e., mixtures with the same two components of various combinations), the upper and the lower bounds can be defined by particle packing theory (Chang and Deng, 2020; De Larrard, 1999; Furnas, 1931; Westman and Hugill, 1930). The void ratios of the binary mixtures with various f_c are between the upper and the lower bounds as the curve ADB shown in Fig. 9a. The packing potential index Ω is defined as the ratio of area ADB to area ACB, which is a material descriptor for a system of mixtures (Chang and Deng, 2020). This index is a measure of volume reduction potential due to mixing of two components of a binary mixture system under a packing procedure, which is a simple scalar and can be directly obtained from experimental data. The value of packing potential index Ω is between 0 and 1. The higher value of Ω indicates a higher potential of volume reduction of the mixtures.

The packing potential indices of the three density states (e_{cs}, e_{max} and e_{min}) for the four particle size ratios are plotted in Fig. 9b. It is interesting to observe that, for each size ratio, the values of these packing potential indices (Ω_{cs}, Ω_{max}, and Ω_{min}) are nearly identical for the three density states (e_{cs}, e_{max}, and e_{min}). The value of Ω seems to be affected mainly by the composition of a mixture but affected marginally by the mechanical procedures that leads to the three density states. It implies that fines content plays the same role in the reduction of void ratio of a binary mixture for these three density states. This particular feature is useful for predicting the critical void ratios as a function of particle size ratio and fines content.

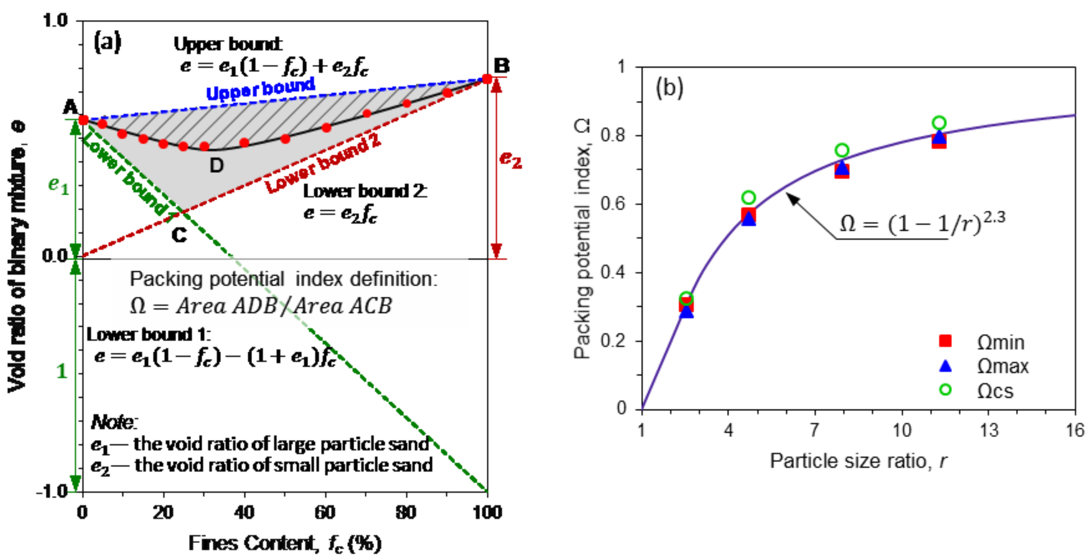

Fig. 9. (a) The definition of packing potential index and (b) packing potential indices for the void ratios of a system of mixtures at three density states.

4.3 Critical state friction angle

The influence of fines content on critical state friction angle ϕ_{cv} were presented in Fig. 10. There are three regions:

(a) For low fines content, ϕ_{cv} of binary mixtures keep close to that of the large particle sand and are almost independent on fines content. This could be because the resistance at critical state for these fines contents is dominated by the contacts between large particles while small particles located in the voids are inactive.

(b) For high fines content, ϕ_{cv} of binary mixtures keep close to that of the fine sand and are also almost independent on fines content. This could be because the resistance at critical state for these fines contents is dominated by the contacts between small particles while large particles embedding in the matrix formed by small particles.

(c) The third region is a transition region. ϕ_{cv} of binary mixtures is a transition value from ϕ_{cv} of the large particle sand to ϕ_{cv} of the fine sand. In the transition region, with increasing fines content, the resistance of a binary mixture at critical state is initially dominated from large particle-to-large particle contacts, transition to large particle-to-small particle contacts, and finally to small particle-to-small particle contacts.

It is noted that in Fig. 8, the transitional fines content is defined as a point (reverse of behaviour). Now, in Fig. 10, there is no abrupt change of behaviour for critical state friction angle; instead, the behaviour change is gradual. Thus, we define a transition region between the lower transitional fines content and the upper transitional fine content.

As shown in Fig. 10, the lower and upper transitional fines contents and the width of transition region vary with different particle size ratio. Particle size ratio might be a key factor controlling transition region, as suggested by Ueda et al. (2011).

As shown in Fig. 10, the transition occurs at lower fines contents with smaller particle size ratios. The reason might be that at smaller particle size ratios the fine particles are too large to fit in the voids between large particles, consequently the network of large particles is altered by the filled fine particles. Thus, the resistance of the binary mixture begin to be dominated by the contacts between large particle-to-small particle at lower fines contents, as suggested by Shire et al. (2014). Therefore, the transition occurs at lower fines contents. At larger particle size ratios, on the contrary, the fines fit well in the voids between large particles, consequently the network of large particles is not altered until the voids are fully filled up. Therefore, the transition occurs at higher fines content for the large particle size ratios compared to that for the small particle size ratios.

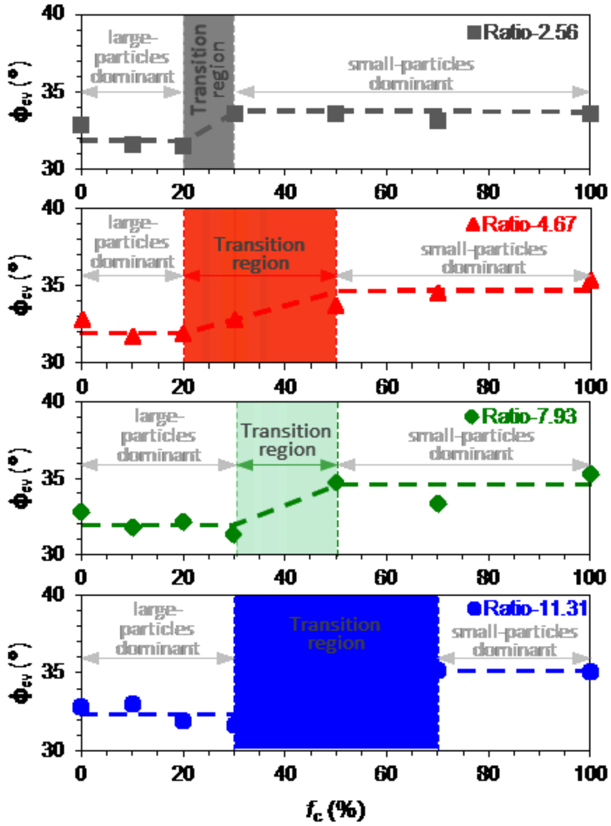

Fig. 10. The influence of fines content on critical state friction angles of binary mixtures with four different particle size ratios.

This transitional behaviour of critical state friction angle varying with fines content is consistent with the influence of fines content on residual friction angle in experimental investigations (Polito and Sibley, 2020; Vallejo, 2001) and in the discrete element (DEM) simulation by Ueda et al., (2011) for simple and direct shear tests.

However, it was observed from other DEM simulations that the critical state friction angle is roughly independent of fines content and particle size ratio (Zhu et al., 2020) and independent of the particle size distribution (Azéma et al., 2017; Yan and Dong, 2011). The experimental investigation on glass beads also showed the grading independence by Harehdasht et al. (2017).

The independence of fine content on ϕ_{cv} could be caused by the fact that the two particle components in a system of mixtures have the same critical state friction angle. In DEM simulation, the particles normally have identical shape, stiffness, and inter-particle coefficient of friction. These identical properties for the two components cause the ϕ_{cv} to be independent of fines content. But, in the DEM simulation by Ueda et al., (2011), the inter-particle coefficients of friction are assigned to be different for the two components, which cause the friction angle to be dependent of fines content. In our tests, the two particle components in a system of mixtures have different critical state friction angles due to the difference in particle angularity. The finer component is a bit more angular than the coarser component and therefore the ϕ_{cv} is higher for pure fines than pure coarse particles. Hence, the value of ϕ_{cv} is dependent on fines content in our test results.

4.4 Maximum dilation angle and peak friction angle

The dilation angle (ψ) was calculated using the following relationship proposed by Vermeer and de Borst (1984):

$$\sin\psi = \frac{-(d\varepsilon_v/d\varepsilon_a)}{2-(d\varepsilon_v/d\varepsilon_a)} \quad (1)$$

The results of maximum dilation angle ψ_p were presented in Fig. 11a. It was observed that fines content has significant influence on ψ_p, especially for the larger particle size ratios, i.e., Ratio-4.67, Ratio-7.93, and Ratio-11.31. For these three particle size ratios, the relationship between ψ_p and fines content has an obvious change around f_c = 30%: ψ_p decreases with an increase in fines content for f_c < 30%, while ψ_p increases with an increase in fines content for f_c > 30%. The smallest ψ_p occurred at the fines content of 30%. For the Ratio-2.56 results, the relationship between ψ_p and fines content is different from those of other three ratios. ψ_p decreases with an increase in fines content for f_c < 20%. The smallest ψ_p occurred at the fines content of 20%. For f_c > 20%, ψ_p increases with an increase in fines content in general except for f_c = 70%.

No obvious trend was observed for the particle size ratio effect on ψ_p for f_c < 30%. However, some trends were observed for $f_c \geq$ 30%. At f_c = 30%, ψ_p decreases with an increase in particle size ratio. The trend evolves and becomes opposite when f_c is above 50%, in which, ψ_p increases with an increase in particle size ratio.

The mechanism of the abovementioned behaviour will be discussed in the later section.

The results of peak friction angle ϕ_p were presented in Fig. 11b. For all particle size ratios, at low fines content, ϕ_p decreases slightly with increasing fines content. With further increasing fines content, ϕ_p is in transition to approach the ϕ_p of the small particle size sand. But the trend for the effect of particle size ratio on the value of ϕ_p was not found.

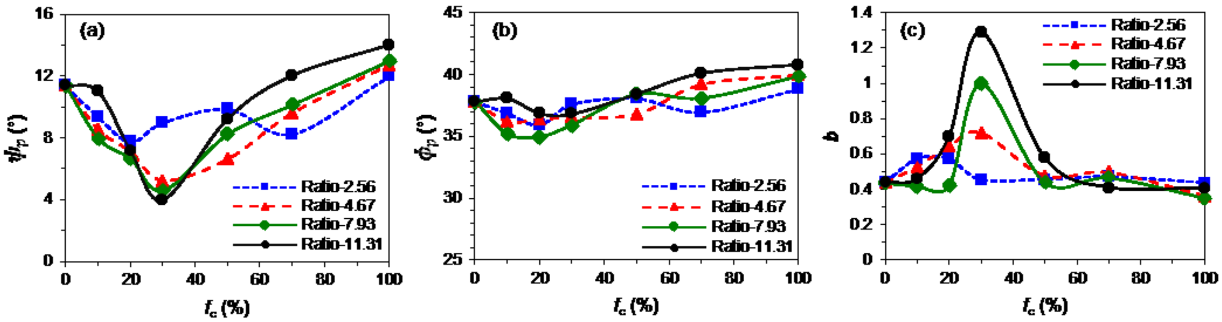

Fig. 11. The influence of fines content on: (a) the maximum dilation angle ψ_p, (b) the peak friction angle ϕ_p, and (c) the dilatancy parameter b in Bolton's stress-dilatancy relation, for binary mixtures with four different particle size ratios.

Bolton (1986) has proposed an empirical formulation to describe the stress-dilatancy relation given by:

$$\phi_p = \phi_{cv} + b\psi_p \quad (2)$$

where parameter b is dilatancy parameter which implies the contribution of dilatancy to the peak strength. The values of b were calculated using the above equation and presented in Fig. 11c. There is little variation in the values of b at low or high fines content, which is consistent with the statement made by Xiao et al. (2017) that the effect of f_c on the value of b is negligible. However, Xiao et al. (2017) observed only on their data of Fujian sand mixtures for $f_c \leq 20\%$. Fig. 11c clearly shows that in the transitional fines content region (around 30%), values of b are much greater than that in low and high fines content regions, and increase with increasing particle size ratio. The large values of b show that the contribution of dilatancy to the peak strength is different between the transitional f_c region and the other two f_c regions. The different contribution of dilatancy to the peak strength indicated that the mechnisms of dilatancy must be different between the transitional f_c region and the other two f_c regions, which will be discussed in the following section.

4.5 Transitional fines content

The transitional fine content is different for different soil behaviour. The transitional fines contents of Silica sand are listed in Table 4 for e_{min}, e_{max}, e_{cs}, ϕ_{cv}, ψ_p, and parameter b.

For e_{min}, e_{max}, e_{cs}, and ψ_p, the curves of the evolutions with fines content are generally V-shape, and the lowest points were selected as transitional fines contents. However, for some curves, the V-shape characteristic is blunt. In this case, a transitional fines content region is estimated, in which the lowest point is located.

For ϕ_{cv}, the curves do not have the V-shape characteristic (see Fig.10). The shape of curves is two steps connected by a ramp. The curve changes gradually from a coarse-particle dominant behaviour to a fine-particle dominant behaviour. Thus, we define a transition region between the lower transitional fines content and the upper transitional fine content as listed in Table 4.

For parameter b, Fig. 11c clearly shows that in the transitional fines content region (around 30%), values of b are much greater than that in low and high fines content regions, and increase with increasing particle size ratio. In this transitional region, the behaviour is very different from those in other regions. The transitional regions were estimated and listed in Table 4.

Table 4 shows that the transitional fines content is dependent on the type of soil behaviour. There is no unique transitional fines content can be defined for a binary mixture.

Table 4 The transitional fines contents f_{th} for different soil behaviours with different particle size ratios.

Soil beahviour	f_{th}	f_{th}	f_{th}	f_{th}
	Ratio-2.56	Ratio-4.67	Ratio-7.93	Ratio-11.31
e_{min}	30%-50%	20%-50%	30%	30%
e_{max}	30%-50%	30%-50%	30%	30%
e_{cs}	20%-50%	30%	30%	30%
ϕ_{cv}	20%-30%	20%-50%	30%-50%	30%-70%
ψ_p	20%	30%	30%	30%
b	10%-30%	20%-50%	20%-50%	20%-50%

5. Discussion on the mechanism for the influences of fines content and particle size ratio on drained shear behaviour

A dense uniform sand sample shearing to critical state successively experiences hardening process and softening process, in which a shear band is usually occurred. The mechanism ending up with the formation of shear bands is the buildup of particle columns during the hardening process and its collapse during the softening process (Iwashita and Oda, 2000).

According to Iwashita and Oda (2000), in the hardening process up to failure, particles are rearranged in chains to form particle columns aligned in the direction of the major principal stress axis, and the applied load is mainly transmitted through them in the form of force chains. As shown in Fig 12a, during the loading process, the pre-existing contacts are lost in the minor principal stress direction, but new contacts are formed in the major principal stress direction. Consequently, an elongated void is generated between two neighboring columns. This is the mechanism causing dilatancy before failure. Due to the forming of particle columns and the elongated void parallel to the major principal stress direction, the packing structure becomes highly anisotropic. Such anisotropic structure becomes gradually unstable because of the loss of surrounding contact points. Finally, the particle columns are collapsed via buckling, as shown in Fig. 12b. The number of buckled columns increases during the loading process, which eventually leads to a peak stress failure. After peak stress, a new packing structure is re-constructed during the softening process. The main process now is the continuing buckling of particle columns gradually concentrated in a narrow shear band, which causes the growth of large voids between buckling columns and particle rotation. Finally, the structure reaches a dynamically stable condition at the critical state. During critical state, buildup and collapse of particle columns keep equilibrium within persistent shear bands. The dilatancy is balanced with the contraction so that the overall volumetric strain remains unchanged, resulting in a constant void ratio.

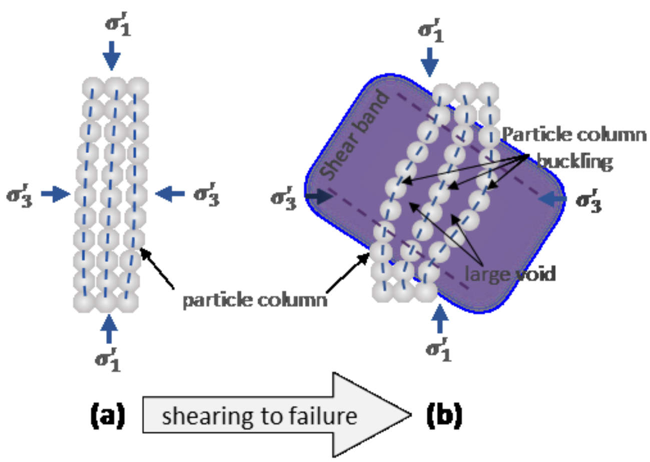

Fig. 12. A schematic diagram illustrating the mechanism for dilatancy: (a) buildup of particle columns and (b) buckling particle columns.

The mechanism for influences of fines content and particle size ratio could be explained from the perspective of particle column buckling, as illustrated in Fig. 13.

For large particle dominant binary mixtures (i.e. at low f_c), as illustrated in Fig 13a, the particle columns are mainly formed by large particles during the hardening process. Small particles are filled between two neighboring columns. Small particles laterally support the particle column to suppress buckling. Consequently, the generation of the elongated void between two neighboring columns is limited. As the elongated void leads to dilatancy before failure, therefore, the dilatancy in the binary mixture is smaller than that in the uniform large particle sand. Increasing fines content further suppress dilatancy, consequently results in a decrease of the maximum dilation angle as shown in Fig. 10a. Although the lateral support provided by the small particles makes the columns more difficult to buckle, at large strain, the columns are still buckled and concentrated within a shear band, which exhibits a localised failure.

For the binary mixtures with a transitional fines content (i.e. f_c is around 30%), as illustrated in Fig 13b, there could be fewer contacts between large-particles owing to being surrounded by small-particles. On the other hand, small particles are not yet enough to form a matrix. As a result, both large and small particle columns cannot be built up during the hardening process. At this f_c, the dilatancy may mainly be caused by particle rearrangement and overriding each other during shearing process. Hence, a smaller level of dilatancy is expected comparing to that induced by column buckling. Since the dilatancy is caused by the overriding of particles, the level of dilatancy is proportional to the size of particles. Therefore, the smallest dilatancy was observed in Ratio-11.31 test with f_c = 30%, compared with the other three ratios with this f_c (see Fig. 11a). Because there are no buckling particle columns, shear band formation is not as visible during the softening process. As a result, we observed that a diffuse-type failure is exhibited instead of a localised failure shown in Fig. 13b.

For small particle dominant binary mixtures (i.e. at high f_c), a matrix is formed by small particles and large particles are floated into it, as illustrated in Fig 13c. During the hardening process, the particle columns are formed by small particles. Large elongated voids causing dilatancy gradually grow between two buckling small particle columns. The number of small particle columns increases with increasing f_c. Therefore, the dilatancy also increases with increasing f_c. Similar to large particle dominant binary mixtures, small particle dominant binary mixtures exhibit a localised failure because buckling particle columns are eventually concentrated within a shear band.

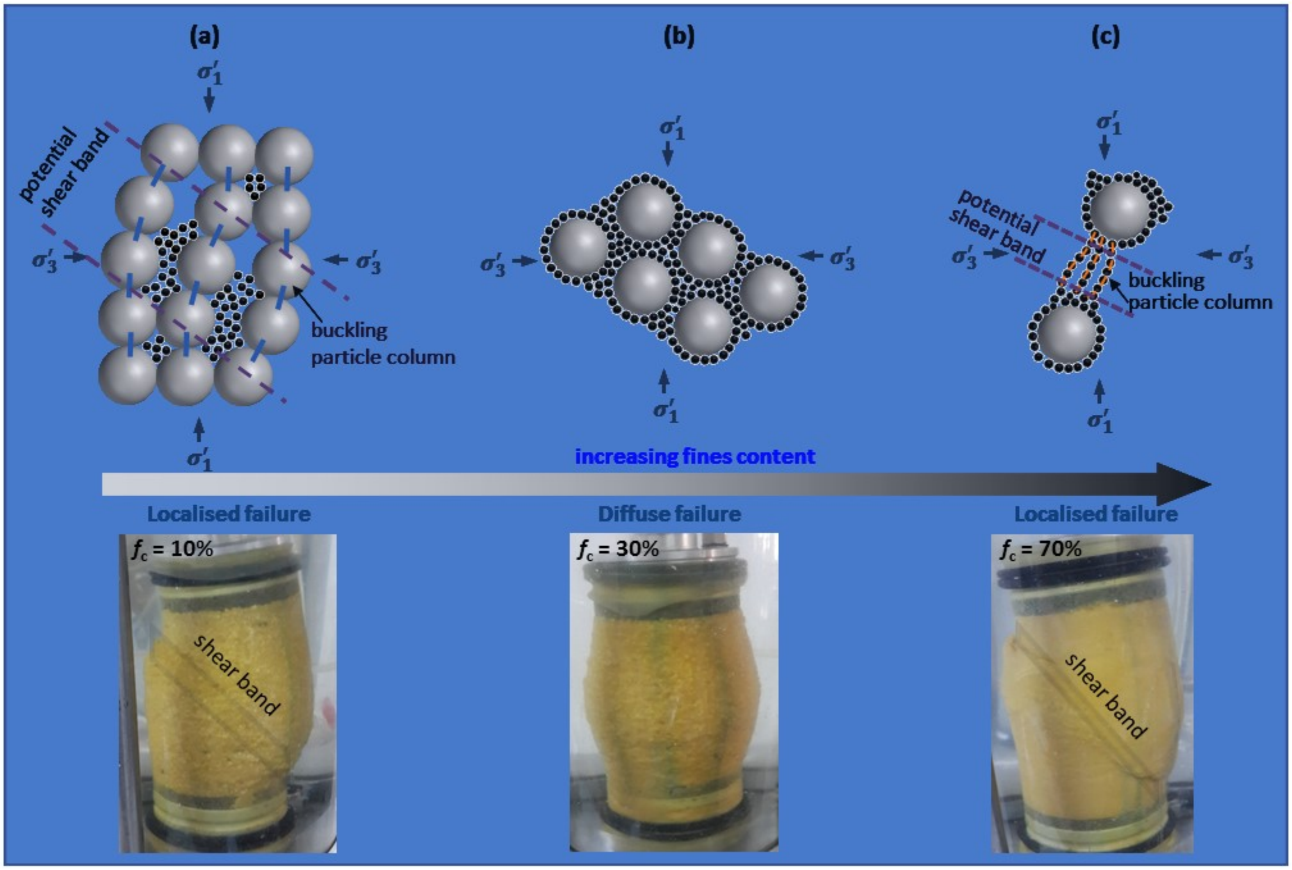

Fig. 13. The mechanisms for dilatancy and failure of binary sand mixtures in: (a) low fines content region, (b) transitional fines content region, and (c) high fines content region.

As shown in Fig. 11a, the uniform sand with smaller particle size has a higher maximum dilation angle, which was consistent with the observations on glass beads and Peribonka sand reported by Harehdasht et al. (2017). Harehdasht et al. (2017) has attributed the increase of dilation angle to the particle size effect. In the silica sand used in this study, the particle roundness generally increases with particle size, thus the effect is caused by both factors of particle size and particle roundness.

At very high f_c, the packing structure for the binary sand mixture is nearly the same as that of uniform fine-sand. Therefore, in this case, higher maximum dilation angle was observed for a mixture with larger particle size ratio (i.e. smaller size particle is more angular in shape) (see Fig. 11a).

As discussed above, the mechanism for dilatancy in the transitional fines content region is different from that in the regions of low and high fines content. Dilatancy in the transitional fines content region is governed by particle rearrangement and overriding each other, while dilatancy in the regions of low and high fines content is governed by the buckling columns. Therefore, as shown in Fig. 11c, the values of b, implying the contribution of dilatancy to the peak strength, are clearly different between the transitional f_c region and the other f_c regions.

Conclusions

In this paper, the effects of fines content and particle size ratio on the drained shear behaviours were studied through a series of drained triaxial compression tests on dense binary silica sand mixtures with 4 different particle size ratios. The critical state and the strength-dilatancy behaviour were analyzed. The mechanism for the effects of fines content and particle size ratio on drained shear behaviour was illustrated. Based on this study the major conclusions can be drawn as follows.

(1) It was observed that when $f_c < f_{th}$, increasing f_c suppresses dilation, on the other hand, when $f_c > f_{th}$, increasing f_c promote dilation.

(2) It was observed that, for high f_c samples, increasing particle size ratio intensifies the post peak softening of the stress-strain curves (i.e., brittle characteristic). For low f_c samples, however, increasing particle size ratio has little influence on the degree of post peak softening of the stress-strain curve.

(3) Both fines content and particle size ratio have significant influence on critical state void ratio. It is interesting to note that the pattern of critical state void ratio is similar to that on minimum and maximum void ratios influenced by particle size ratio. The similar pattern might imply that fines content plays the same role in the reduction of void ratio of a binary mixture for these three density states.

(4) The value of ϕ_{cv} of a mixture is influenced by its fines content, which can be divided in 3 regions: (a) at low fines content region, the ϕ_{cv} values of binary mixtures are close to the ϕ_{cv} of large particles; (b) at high fines content region, the ϕ_{cv} values of binary mixtures are close to the ϕ_{cv} of fine particles; (c) in the transition region, the ϕ_{cv} values of binary mixtures are transition from the ϕ_{cv} of the large particle sand to the ϕ_{cv} of the fine sand.

(5) A general trend for the effect of fines content on ψ_p is observed. ψ_p decreases with an increase in fines content for $f_c < 30\%$. But, ψ_p increases with an increase in fines content for $f_c > 30\%$. The smallest ψ_p occurred at the fines content of 30%. No obvious trend was observed for the particle size ratio effect on ψ_p for $f_c < 30\%$. However, at $f_c = 30\%$, there is a clear trend that ψ_p decreases with an increase in particle size ratio. The trend evolves and becomes opposite when f_c is above 50%, in which, ψ_p increases with an increase in particle size ratio.

(6) It was found that the parameter b in Bolton' stress-dilatancy relation has a little variation in low and high fines content regions. In the transitional fines content region, however, the parameter b is much greater than that in the other two regions and increase with increasing particle size ratio.

(7) The mechanism was proposed to illustrate the influences of fines content and particle size ratio on the drained shear behaviour from the perspective of particle column buckling. Dilatancy in the transitional region of fines content is governed by the rearrangement of particle, which override each other. Whereas, dilatancy in the regions of low or high fines content is governed by the buckling of particle columns. The influences of fines content and particle size ratio on dilatancy and value of b in the Bolton's stress–dilatancy equation were explained by the proposed mechanism. The mechanism explained in this paper is only a conjecture, which cannot be verified by triaxial tests alone. It needs to be further verified by other analysis such as DEM simulation.

Acknowledgement

This work was supported by the National Science Foundation of the United States under a research grant (CMMI-1917238). The support is greatly acknowledged.

Appendix A: Examples to determine the critical state

A.1 For samples without visualized localisation at large strain

For a sample without visualized deformation localisation, we assume that localisation is minute and the deformation is relatively uniform for the range of stress-strain curve between the peak stress and the end of test, which can be used to assess the critical state.

The critical state was determined by an extrapolating method described herein. The sample with Ratio-4.67 at 30% f_c was taken as an example shown in Fig. A.1. The critical state friction angle was firstly estimated with a stress-dilatancy analysis as shown in Fig. A.1a. In this analysis, the Nova's stress-dilatancy relationship (Nova, 1982) was used to fit the stress-dilatancy data of post-peak stress,

$$\eta = M + (1 - N)D \tag{A.1}$$

where M is the stress ratio at critical state and N is a volumetric coupling coefficient. After the values of M and N were obtained from fitting the data, the critical state friction angle ϕ_{cv} was then obtained using the relationship $sin\phi_{cv} = 3M/(6 + M)$ and listed in Table 3.

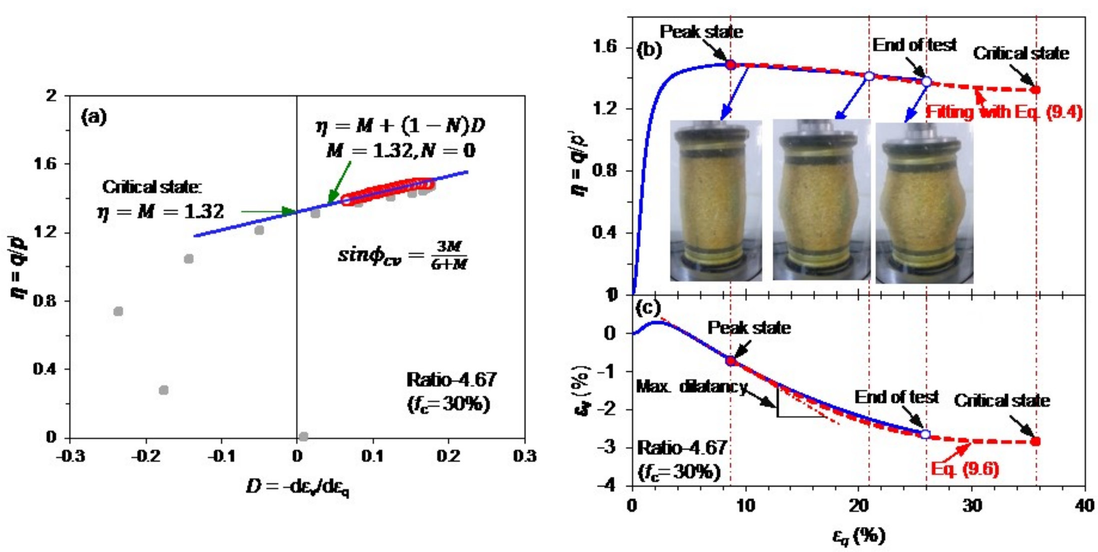

Fig. A.1. An example of extrapolating the data to determine the critical state for a sample without visualized localisation: (a) stress-dilatancy analysis, (b) extrapolated stress-strain curve, and (c) extrapolated volumetric strain curve.

For convenience, a cosine function was used to extrapolate the post-peak stress-strain curve.

$$\eta = \frac{\eta^{peak}+M}{2} + \frac{\eta^{peak}-M}{2} cos\left(\frac{\varepsilon_q-\varepsilon_q^{peak}}{\varepsilon_q^{cs}-\varepsilon_q^{peak}} \cdot \pi\right);\ \varepsilon_q \in [\varepsilon_q^{peak}, \varepsilon_q^{cs}] \tag{A.2}$$

where the superscripts 'peak' and 'cs' denote for peak state and critical state, respectively. Fig. A.1b and Fig A.2a show that this cosine function is satisfactory to express the post-peak stress-strain curves. The deviator strain ε_q^{cs}, where the critical state occurs, was estimated by a regression analysis performed on the stress-strain data from the peak stress to the end of the test. The regression analysis minimizes the sum of squared errors *SS,*

$$SS(\varepsilon_q^{cs}) = \sum_i \left[\eta^i - \eta(\varepsilon_q^i, \varepsilon_q^{cs})\right]^2 \tag{A.3}$$

where η^i and ε_q^i are the measured i^{th} point on the stress-strain curve. Substituting Eq. (A.2) into Eq. (A.1) and then integrating with respect to ε_q, the expression of volumetric strain ε_v as a function of ε_q between peak state and critical state was obtained as follows

$$\varepsilon_v = \frac{M-\eta^{peak}}{2(1-N)} \cdot \left[\left(\varepsilon_q - \varepsilon_q^{peak}\right) + \frac{\varepsilon_q^{cs}-\varepsilon_q^{peak}}{\pi} sin\left(\frac{\varepsilon_q-\varepsilon_q^{peak}}{\varepsilon_q^{cs}-\varepsilon_q^{peak}} \cdot \pi\right)\right] + \varepsilon_v^{peak} \tag{A.4}$$

As shown in Fig. A.1c and Fig A.2b, Eq. (A.4) matches the measured results well and can be used to extrapolate the curve of volumetric change response. Using this extrapolation method, the critical state void ratios for the samples without visualized deformation localisation were determined and listed in Table 3.

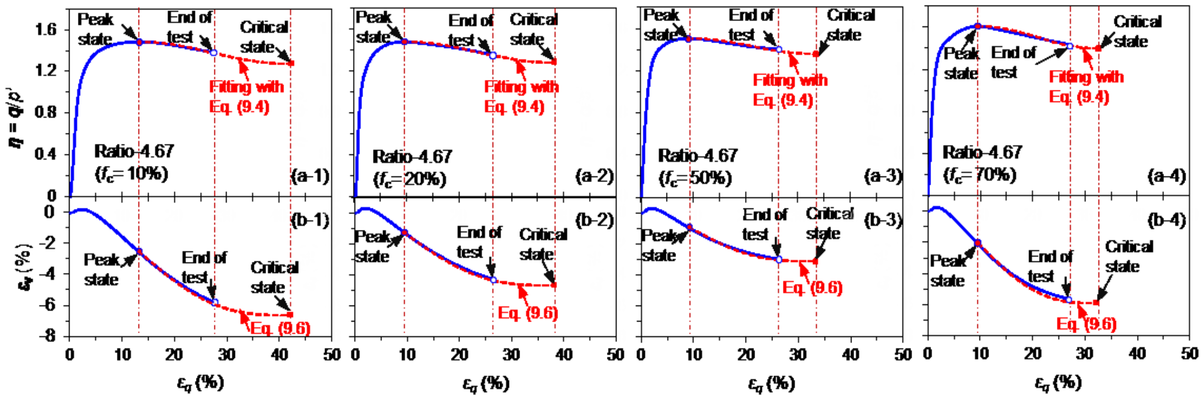

Fig. A.2. Examples of extrapolating the data to determine the critical state for four samples of binary mixtures without visualized localisation: (a) extrapolated stress-strain curve and (b) extrapolated volumetric strain curve.

A.2 For samples with visualized localisation at large strain

The sample deformation after the occurrence of localisation is not representative of a uniformly deformed material thus cannot be used for extrapolation. Thus, for a sample with visualized localisation, the critical state needs to be determined by using multiple test results (Harehdasht et al., 2017; Nova, 1982). In this study, we use test results from three different confining stresses (i.e., 100 kPa, 200 kPa, and 400 kPa). Assuming that the occurred localisation is minute at peak stress state, the critical state stress ratio M was obtained by fitting the peak points of three stress-dilatancy curves using Eq. (A.1) as shown in Fig. A.3a. After the stress-dilatancy relationship for each sample was obtained, the critical state friction angle ϕ_{cv} was then obtained using the relationship $sin\phi_{cv} = 3M/(6+M)$ and listed in Table 3.

The initiation of localisation begins at peak stress state. The localisation becomes prominent after a point of maximum curvature, at which the stress strain curve deviates from the smooth curve. After this point, a greater softening commences. The minute localisation propagates into a visualized shear band with abrupt stress reduction (see Fig. A.3b). We assume that localisation is ineffective and the deformation is relatively uniform for the range of stress-strain curve between the peak stress and the point of maximum curvature. This portion of measured curve can be used to assess the critical state.

As discussed previously, the post-peak stress-strain curve without visualized localisation can be expressed by a cosine function (Eq. A.2). Hence, this cosine function was also used to extrapolate the stress-strain curve between the peak stress and the point of maximum curvature for the samples with visualized deformation localisation. Using Eq. (A.2) with the determined M from three test results, the critical state deviator strain ε_q^{cs} was estimated by a regression analysis performed on the stress-strain data from the peak stress to the point of maximum curvature. The examples of the extrapolating stress-strain curves are shown in Fig. A.3b. The expression of volumetric strain ε_v as a function of ε_q between peak state and critical state was obtained based on the established stress-dilatancy relationship and the estimated ε_q^{cs}. The examples of the extrapolating volumetric strain curves are shown in Fig. A.3c. Using this extrapolation method, the critical state void ratios for the samples with visualized localisation were determined and listed in Table 3.

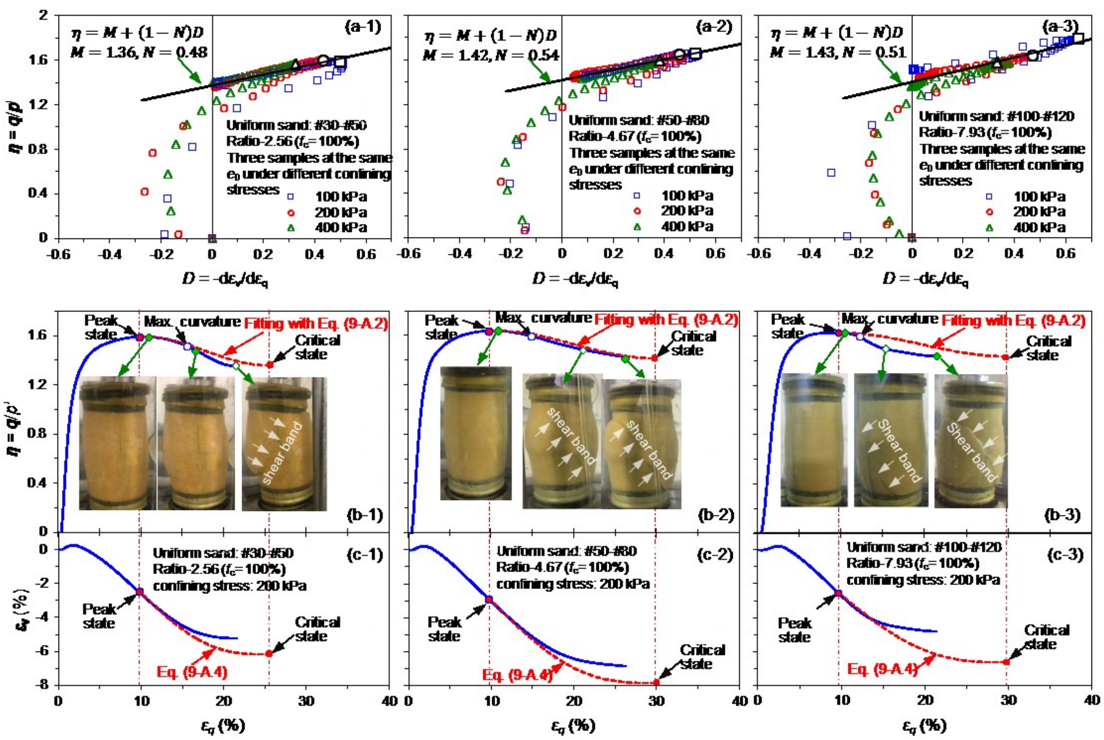

Fig. A.3. Examples of extrapolating the data to critical state for the samples with deformation localisation: (a) stress-dilatancy analysis, (b) extrapolated stress-strain curve, and (c) extrapolated volumetric strain curve.

References

ASTM D4253-00, 2006. Standard test methods for maximum index density and unit weight of soils using a vibratory table, in: Annual Book of ASTM Standards. ASTM International, West Conshohocken, PA, pp. 1–15. https://doi.org/10.1520/D4253-00R06.

ASTM D4254-00, 2006. Standard Test Methods for Minimum Index Density and Unit Weight of Soils and Calculation of Relative Density, in: Annual Book of ASTM Standards. ASTM International, West Conshohocken, PA, pp. 1–9. https://doi.org/10.1520/D4254-00R06E01.1.3

Azéma, E., Linero, S., Estrada, N., Lizcano, A., 2017. Shear strength and microstructure of polydisperse packings: The effect of size span and shape of particle size distribution. Phys. Rev. E 96, No. 2, 022902. https://doi.org/10.1103/PhysRevE.96.022902

Been, K., Jefferies, M., 2004. Stress-dilatancy in very loose sand. Can. Geotech. J. 41, 972–989. https://doi.org/10.1139/t04-038

Bolton, M.D., 1986. The strength and dilatancy of sands. Géotechnique 36, No. 1, 65–78. https://doi.org/10.1680/geot.1986.36.1.65

Bouckovalas, G.D., Andrianopoulos, K.I., Papadimitriou, A.G., 2003. A critical state interpretation for the cyclic liquefaction resistance of silty sands. Soil Dyn. Earthq. Eng. 23, No. 2, 115–125. https://doi.org/10.1016/S0267-7261(02)00156-2

Carraro, J.A.H., Prezzi, M., Salgado, R., 2009. Shear strength and stiffness of sands containing plastic or nonplastic fines. J. Geotech. Geoenvironmental Eng. 135, no. 9, 1167–1178. https://doi.org/10.1061/(ASCE)1090-0241(2009)135

Carrera, A., Coop, M., Lancellotta, R., 2011. Influence of grading on the mechanical behaviour of Stava tailings. Géotechnique 61, No. 11, 935–946. https://doi.org/10.1680/geot.9.P.009

Chang, C.S., Deng, Y., 2020. Packing potential index for binary mixtures of granular soil. Powder Technol. 372, 148–160. https://doi.org/10.1016/j.powtec.2020.06.005

Chang, C.S., Meidani, M., 2013. Dominant grains network and behavior of sand–silt mixtures: stress–strain modeling. Int. J. Numer. Anal. Methods Geomech. 37, 2563–2589. https://doi.org/10.1002/nag.2152

Chang, C.S., Yin, Z.Y., 2011. Micromechanical modeling for behavior of silty sand with influence of fine content. Int. J. Solids Struct. 48, No. 19, 2655–2667. https://doi.org/10.1016/j.ijsolstr.2011.05.014

Chang, W., Phantachang, T., 2016. Effects of gravel content on shear resistance of gravelly soils. Eng. Geol. 207, May, 78–90. https://doi.org/10.1016/j.enggeo.2016.04.015

Dash, H.K., Sitharam, T.G., 2011. Undrained monotonic response of sand–silt mixtures: effect of nonplastic fines. Geomech. Geoengin. 6, No. 1, 47–58. https://doi.org/10.1080/17486021003706796

De Larrard, F., 1999. Concrete Mixture Proportioning: A scientific approach. E & FN SPON, London,UK.

Derkaoui, M., Missoum, H., Bendani, K., Belhouari, F., 2016. Shear Behavior of Sand–Silt Mixtures: A Laboratory Investigation of Coastal Silty Sand Soils of Mostaganem. Mar. Georesources Geotechnol. 34, No. 7, 668–680. https://doi.org/10.1080/1064119X.2015.1070388

Furnas, C.C., 1931. Grading aggregates I: Mathematical relations for beds of broken solids of maximum density. Ind. Eng. Chem. 23, No. 9, 1052–1058. https://doi.org/10.1021/ie50261a017

Harehdasht, S.A., Karray, M., Hussien, M.N., Chekired, M., 2017. Influence of Particle Size and Gradation on the Stress-Dilatancy Behavior of Granular Materials during Drained Triaxial Compression. Int. J. Geomech. 17, No. 9, 04017077. https://doi.org/10.1061/(ASCE)GM.1943-5622.0000951.

Huang, Y.-T., Huang, A.-B., Kuo, Y.-C., Tsai, M.-D., 2004. A laboratory study on the undrained strength of a silty sand from Central Western Taiwan. Soil Dyn. Earthq. Eng. 24, No. 9, 733–743. https://doi.org/10.1016/j.soildyn.2004.06.013

Indraratna, B., Nimbalkar, S., Coop, M., Sloan, S.W., 2014. A constitutive model for coal-fouled ballast capturing the effects of particle degradation. Comput. Geotech. 61, 96–107. https://doi.org/10.1016/j.compgeo.2014.05.003

Iwashita, K., Oda, M., 2000. Micro-deformation mechanism of shear banding process based on modified distinct element method. Powder Technol. 109, 192–205.

Jehring, M.M., Bareither, C.A., 2016. Tailings composition effects on shear strength behavior of co-mixed mine waste rock and tailings. Acta Geotech. 11, No. 5, 1147–1166. https://doi.org/10.1007/s11440-015-0429-1

Kwa, K.A., Airey, D.W., 2016. Critical state interpretation of effects of fines in silty sands. Géotechnique Lett. 6, No. 1, 100–105. https://doi.org/10.1680/jgele.15.00176

Kwan, A.K.H., Chan, K.W., Wong, V., 2013. A 3-parameter particle packing model incorporating the wedging effect. Powder Technol. 237, 172–179. https://doi.org/10.1016/j.powtec.2013.01.043

Ladd, R.S., 1978. Preparing test specimens using undercompaction. Geotech. Test. J. 1, No. 1, 16–23.

Li, X.S., Dafalias, Y.F., 2000. Dilatancy for cohesionless soils. Geotechnique 50, No. 4, 449–460. https://doi.org/10.1680/geot.2000.50.4.449

McGeary, R.K., 1961. Mechanical Packing of Spherical Particles. J. Am. Ceram. Soc. 44, No. 10, 513–522. https://doi.org/10.1111/j.1151-2916.1961.tb13716.x

Murthy, T.G., Loukidis, D., Carraro, J.A.H., Prezzi, M., Salgado, R., 2007. Undrained monotonic response of clean and silty sands. Géotechnique 57, No. 7, 273–288. https://doi.org/10.1680/geot.2007.57.3.273

Naeini, S.A., Baziar, M.H., 2004. Effect of fines content on steady-state strength of mixed and layered samples of a sand. Soil Dyn. Earthq. Eng. 24, No. 3, 181–187.

Ni, Q., Tan, T.S., Dasari, G.R., Hight, D.W., 2004. Contribution of fines to the compressive strength of mixed soils. Geotechnique 54, No. 9, 561–569.

Nova, R., 1982. A constitutive model under monotonic and cyclic loading, in: Pande, G., Zienkiewicz, O.C. (Eds.), Soil Mechanics — Transient and Cyclic Loads. John Wiley & Sons Ltd., New York, USA, pp. 343–373.

Papadopoulou, A., Tika, T., 2008. The effect of fines on critical state and liquefaction resistance characteristics of non-plastic silty sands. Soils Found. 48, No. 5, 713–725. https://doi.org/10.3208/sandf.47.887

Patil, U.D., Hoyos, L.R., Puppala, A.J., Bheemasetti, T.V., 2018. Modeling Stress – Dilatancy Behavior of Compacted Silty Sand Under Suction-Controlled Axisymmetric Shearing. Geotech. Geol. Eng. 36, No. 6, 3961–3977. https://doi.org/10.1007/s10706-018-0647-z

Polito, C.P., Sibley, E.L.D., 2020. Threshold fines content and behavior of sands with nonplastic silts. Can. Geotech. J. 57, No. 3, 462–465. https://doi.org/10.1139/cgj-2018-0698

Rahman, M.M., Lo, S.-C.R., Dafalias, Y.F., 2014. Modelling the static liquefaction of sand with low-plasticity fines. Ge´otechnique 64, No. 11, 881–894. https://doi.org/10.1680/geot.14.P.079

Roscoe, K.H., Schofield, A.N., Wroth, C.P., 1958. On the yielding of soils. Geotechnique 1, 22–53.

Salgado, R., Bandini, P., Karim, A., 2000. Shear Strength and Stiffness of Silty Sand. J. Geotech. Geoenvironmental Eng. 126, No. 5, 451–462. https://doi.org/10.1061/(ASCE)1090-0241(2000)126:5(451)

Shire, T., O'Sullivan, C., Hanley, K.J., Fannin, R.J., 2014. Fabric and effective stress distribution in internally unstable soils. Journalof Geotech. Geoenvironmental Eng. 140, No. 2, 04014072. https://doi.org/10.1061/(ASCE)GT.1943-5606.0001184

Thevanayagam, S., Shenthan, T., Mohan, S., Liang, J., 2002. Undrained fragility of clean sands, silty sands, and sandy silts. J. Geotech. Geoenvironmental Eng. 128, No. 10, 849–859. https://doi.org/10.1061/(ASCE)1090-0241(2002)128:10(849)

Ueda, T., Matsushima, T., Yamada, Y., 2011. Effect of particle size ratio and volume fraction on shear strength of binary granular mixture. Granul. Matter 13, No. 3, 731–742. https://doi.org/10.1007/s10035-011-0292-1

Vallejo, L.E., 2001. Interpretation of the limits in shear strength in binary granular mixtures. Can. Geotech. J. 38, No. 5, 1097–1104. https://doi.org/10.1139/t01-029

Vermeer, P.A., de Borst, R., 1984. Non-associated plasticity for soils, concrete and rock. HERON 29, No. 3, 1–64.

Wadell, H., 1935. Volume, Shape, and Roundness of Quartz Particles. J. Geol. 43, No. 3, 250–280.

Wei, X., Yang, J., 2019. Characterizing the effects of fines on the liquefaction resistance of silty sands. Soils Found. 59, No. 6, 1800–1812. https://doi.org/10.1016/j.sandf.2019.08.010

Westman, A.E.R., Hugill, H.R., 1930. The packing of particles. J. Am. Ceram. Soc. 13, No. 10, 767–779. https://doi.org/10.1111/j.1151-2916.1930.tb16222.x

Xiao, Y., Desai, C., 2016. General Stress – Dilatancy Relation for Granular Soils. J. Geotech. Geoenvironmental Eng. 142, No. 4, 2816001. https://doi.org/10.1061/(ASCE)GT.1943-5606.0001473

Xiao, Y., Liu, H., Ding, X., Chen, Y., Jiang, J., Wengang Zhang, 2016. Influence of Particle Breakage on Critical State Line of Rockfill Material. Int. J. Geomech. 16, No. 1, 04015031. https://doi.org/10.1061/(ASCE)GM.1943-5622.0000538

Xiao, Y., Xiang, J., Liu, H., Ma, Q., 2017. Strength-dilatancy relation of sand containing non-plastic fines. Géotechnique Lett. 7, No. 2, 204–210. https://doi.org/10.1680/jgele.16.00144

Yan, W., Dong, J., 2011. Effect of particle grading on the response of an idealized granular assemblage. Int. J. Geomech. ASCE 11, No. 4, 276–285. https://doi.org/10.1061/(ASCE)GM.1943-5622.0000085.

Yang, S., Lacasse, S., Sandven, R., 2006. Determination of the transitional fines content of mixtures of sand and non-plastic fines. Geotech. Test. J. 29, No. 2, 1–6. https://doi.org/10.1520/GTJ14010

Yang, S.L., 2004. Characterization of the properties of sand-silt mixtures. Norwegian University of Science and Technology, Trondheim, Norway.

Yilmaz, Y., 2009. A study on the limit void ratio characteristics of medium to fine mixed graded sands. Eng. Geol. 104, No. 3-4, 290–294. https://doi.org/10.1016/j.enggeo.2008.11.009

Yin, Z.Y., Zhao, J., Hicher, P.Y., 2014. A micromechanics-based model for sand-silt mixtures. Int. J. Solids Struct. 51, No. 6, 1350–1363. https://doi.org/10.1016/j.ijsolstr.2013.12.027

Zhou, W., Xu, K., Ma, G., Yang, L., Chang, X., 2016. Effects of particle size ratio on the macro- and microscopic behaviors of binary mixtures at the maximum packing efficiency state. Granul. Matter 18, 1–13. https://doi.org/10.1007/s10035-016-0678-1

Zhu, Y., Nie, Z., Gong, J., Zou, J., Zhao, L., Li, L., 2020. An analysis of the effects of the size ratio and fines content on the shear behaviors of binary mixtures using DEM. Comput. Geotech. 118, No. 4, 103353. https://doi.org/10.1016/j.compgeo.2019.103353

Zlatovic, S., Ishihara, K., 1995. On the influence of nonplastic fines on residual strength, in: Ishihara, K. (Ed.), Earthquake Geotechnical Engineering. Balkema, Rotterdam, pp. 239–244.

Zuo, L., Baudet, B.A., 2015. Determination of the transitional fines content of sand-non plastic fines mixtures. Soils Found. 55, No. 1, 213–219. https://doi.org/10.1016/j.sandf.2014.12.017

Caption of Figures

Fig. 1. Micrographs of uniform silica sands of five different particle sizes.

Fig. 2. The grain size distributions of binary mixtures with four different particle size ratios: (a) Ratio-2.56, (b) Ratio- 4.67, (c) Ratio-7.93, and (d) Ratio-11.31

Fig. 3. The initial void ratios e_0 of all samples.

Fig. 4. Experimental results of the drained triaxial compression tests on binary mixtures of various fines contents and particle size ratios.

Fig. 5. The stress-dilatancy plots for binary mixtures of various fines contents and particle size ratios.

Fig. 6. The minimum void ratios of binary granular mixtures with various particle size ratios: (a) steel shots and (b) glass beads.

Fig. 7. The critical state void ratios of five different types of sand-silt mixtures with various fines contents.

Fig. 8. The effects of fines content and particle size ratio on (a) critical state void ratio, (b) minimum void ratio, and (c) maximum void ratio.

Fig. 9. (a) The definition of packing potential index and (b) packing potential indices for the void ratios of a system of mixtures at three density states.

Fig. 10. The influence of fines content on critical state friction angles of binary mixtures with four different particle size ratios.

Fig. 11. The influence of fines content on: (a) the maximum dilation angle ψ_p, (b) the peak friction angle ϕ_p, and (c) the dilatancy parameter b in Bolton's stress-dilatancy relation, for binary mixtures with four different particle size ratios.

Fig. 12. A schematic diagram illustrating the mechanism for dilatancy: (a) buildup of particle columns and (b) buckling particle columns.

Fig. 13. The mechanisms for dilatancy and failure of binary sand mixtures in: (a) low fines content region, (b) transitional fines content region, and (c) high fines content region.

Fig. A.1. An example of extrapolating the data to determine the critical state for a sample without visualized localisation: (a) stress-dilatancy analysis, (b) extrapolated stress-strain curve, and (c) extrapolated volumetric strain curve.

Fig. A.2. Examples of extrapolating the data to determine the critical state for four samples of binary mixtures without visualized localisation: (a) extrapolated stress-strain curve and (b) extrapolated volumetric strain curve.

Fig. A.3. Examples of extrapolating the data to critical state for the samples with deformation localisation: (a) stress-dilatancy analysis, (b) extrapolated stress-strain curve, and (c) extrapolated volumetric strain curve.

Caption of Tables

Table 1 Properties of the uniform silica sands of five different particle sizes.

Table 2 List of index properties of tested binary mixtures.

Table 3 Summary results of drained triaxial compression tests on the specimens of binary silica sand mixtures of various fines contents for four different particle size ratios.

Table 4 The transitional fines contents f_{th} for different soil behaviours with different particle size ratios.